Composites Science and Technology 68 (2008) 3047–3054

Contents lists available at ScienceDirect

Composites Science and Technology

journal homepage: www.elsevier.com/locate/compscitech

Spring-in angle as molding distortion for thermoplastic matrix composite

A. Salomi [a,*], T. Garstka [b], K. Potter [b], A. Greco [a], A. Maffezzoli [a]

[a] Department of Innovation Engineering, University of Salento, via Monteroni, 73100 Lecce, Italy
[b] Department of Aerospace Engineering, University of Bristol, Queens Building, University Walk, Bristol BS8 1TR, UK

ARTICLE INFO

Article history:
Received 17 December 2007
Received in revised form 28 May 2008
Accepted 28 June 2008
Available online 4 July 2008

Keywords:
A. Polymer matrix composites
B. Thermo-mechanical properties
C. Anisotropy
E. Laser reflection technique

ABSTRACT

In this work, the spring-in angle behavior of a U-channel shaped thermoplastic matrix laminate is studied. The consolidation of the U-channel shaped profile having two different corner radii took place in an autoclave. Spring-in angle was measured at room temperature, after cooling in the autoclave, and during subsequent heating at different temperatures and after final cooling to room temperature. Different thermally induced spring-in angle behaviors were observed for the two inner radii of U-specimen. Thermal expansion coefficients in the through the thickness and in-plane directions were measured. Experimental spring-in angle data were then compared with a differential model derived from the Radford model. Some differences between the model results and experimental spring-in data were observed. The differences observed between the two radii and between experimental and model results were attributed to the existence of fibers distortion at the corner, leading to significant fibers misalignment and wrinkling. Consequently, the Radford model was modified to account for the increase of thermal expansion coefficient in the through the thickness direction. Results showed a better agreement with experimental data. Finally, the difference observed in the spring-in angle before and after heating of the composite indicates the relevance of non-thermoelastic effects in thermoplastic matrix composites.

1. Introduction

Thermoplastic matrix composites, based on commodity polymers, are attracting increasing interest, essentially thanks to their fast processability, high impact strength, chemical resistance, low moisture absorption, unlimited shelf life of raw materials, and low cost. In addition, the ability of thermoplastic matrix composites to be recycled is one of the main advantages over thermosetting [1–3]. Because of its characteristics of low density, good processability and environmental resistance, isotactic polypropylene (iPP) is considered one of the most suitable thermoplastic matrix candidates for many industrial applications.

During processing of thermoplastic based composites, pressure and temperature are applied to the material to allow fibers impregnation and void fraction reduction [4,5]. At high temperatures, the low viscosity of the polymer and the applied pressure assure adequate flow of the molten phase, which impregnates the fibers [6–8]. During the subsequent cooling stage, crystallization occurs [9,10], forming a consolidated composite. The flow of the molten material is governed by Darcy's law [11–13]. As a consequence of this, low viscosities and low migration distance of the polymer matrix enhance the consolidation step, even in the presence of low applied pressures. A reduced flow distance is usually obtained using commingled yarn composites, which can then be processed at very low pressures. One of the most important problems associated with processing of composite parts is molding distortion. A typical mould distortion for angle shaped parts on cooling is commonly called spring-in. The difference between the in-plane and the through thickness thermal expansion coefficient leads to a reduction of the enclosed angle [14], as shown in Fig. 1. Distortions in thin and flexible components can be ignored because the deformations can be easily corrected during assembly operations. However, in the case of rigid components, such deformations cannot be ignored since they cannot be easily removed during assembly. The most common residual stress effect encountered in manufacturing composites is deformation of angled and curved parts. Currently, tool angles are modified to compensate for part spring-in. The tool geometries is based on either 'rules-of-thumb' from past experience or trial-and-error. For angular parts, the compensation is normally between 1° and 2.5°. The most common problem found in using a standard factor is that the spring-in may vary with lay-up, material, processing temperature, mould geometry etc. [15,16].

Spring-in behavior has been widely studied for thermoset based composites. Many papers indicate that the spring-in behavior depends upon different factors, including material properties, process conditions and composite lay-up [14,17]. The most commonly used approach to study the spring-in behavior of thermoset based composites was developed by Radford [14]. In recent years, other studies have dealt with spring-in angle for thermoplastic matrix composites [18–21]. It is generally accepted that also in the case of thermoplastic matrix composite the spring-in angle is due to

* Corresponding author. Tel.: +39 347 9025799; fax: +39 832 297240.
E-mail address: andreasalomi@yahoo.it (A. Salomi).

0266-3538/$ - see front matter © 2008 Elsevier Ltd. All rights reserved.
doi:10.1016/j.compscitech.2008.06.024

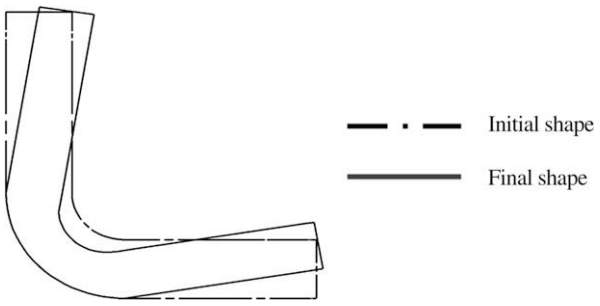

Fig. 1. Spring-in after cooling of a *L*-section composite (fig. by T. Gartska).

different thermal expansion coefficients in the in-plane and through the thickness directions. Further, owing to their long molecular chains, thermoplastics have a high melting temperature, and consequently the processing temperatures are much higher than those typical of thermoset based composites. This contributes to build up of large residual stresses during the cooling stage [18]. Also, for thermoplastic matrix composite, the gradients in cooling rate can result in morphological non-homogeneities in the polymer matrix, particularly in semi crystalline polymers. This effect, which is usually referred to as "skin-core" effect [21] is a further source of anisotropy. For thermoplastic based composites, the evolution of composite stiffness, and of residual stresses, is expected to be different than that observed for thermoset based composites. Thermal distortion can arise, in thermoset based composite processing, during the heating and the cooling stage, after the stiffness develops at the cure temperatures [14,16]. On the other hand, thermal distortion during thermoplastic processing can only take place during the cooling stage after crystallization occurs.

In this work, the dimensional changes of a Polypropylene matrix composite were studied by thermo-mechanical analysis to determine the thermal expansion coefficients of the material both in-plane and through thickness. Spring-in angle of U-shaped laminate at room temperature after processing was measured by a coordinate measuring machine (CMM). The spring-in angle upon heating was measured using a laser measuring system. Experimental results were compared with the analytical model derived by the one developed by Radford and Rennik [14] for thermoset based composites.

2. Experimental

2.1. Materials

The composite laminate used in this work is obtained by consolidation of a commingled woven fabric, Twintex® T PP 60 745 AF 152. The identification of this product are: 2/2 twill balanced fabric (T); isotactic polypropylene matrix (PP); 60% by weight of E-glass and 40% by weight of iPP; 745 g/m^2 as nominal weight; commingled rowing type (AF); 152 cm width; produced by Vetrotex. The unconsolidated fabric is about 1.5 mm in thickness. The material can be consolidated by the combined effect of temperature and pressure in autoclave.

An autoclave Quicklock Thermoclave Leeds and Bradford Boiler Company Limited was used for the production of flat and U-shaped laminates. In both cases, 8-plys of Twintex were stacked, with symmetrical [0/90] sequences, and pre-consolidated on the tool using a nylon 6 vacuum bagging film. Flat specimens, used for the determination of thermal expansion coefficient (CTE), were bagged on a flat aluminum plate. U-channel specimens, used for determination of spring-in angle, were manufactured, with fiber oriented along the channel longitudinal axis, on a female aluminum U-channel shaped tool. In particular the geometric characteristic of the tool is an angle of 92° between each arm and the base of the tool. In order to highlight the effect of corner radius on spring-in angle, inner radii of 16 and 32 mm were used as shown in Fig. 2.

During the thermal cycle in the autoclave a pressure of 6.9 bar was applied on the material. Positive pressure and vacuum were held for the entire thermal cycle (heating and cooling) while the temperature was measured. During the thermal cycle the material was heated at a very low heating rate (0.5 °C/min) up to 180 °C, and then held at constant temperature for 1 h. A faster cooling rate (about 6.5 °C/min) was adopted. The temperature profiles during the heating and cooling cycle in the autoclave are reported in Fig. 3. This optimized thermal cycle was based on previous work in Twintex® molding [22]. An homogeneous heat flow in the composite from the vacuum bag and the mould side results by their comparable thermal resistance. In facts, as reported in Fig. 3, the maximum temperature difference between the mould side and the bag side of the composite is about 3 °C.

Sections of U-channel were cut by diamond saw to obtain the specimens for spring-in testing.

2.2. Thermal expansion coefficient measurement

The thermal expansion coefficient (CTE) of Twintex laminates was measured both in the in-plane and through thickness direction.

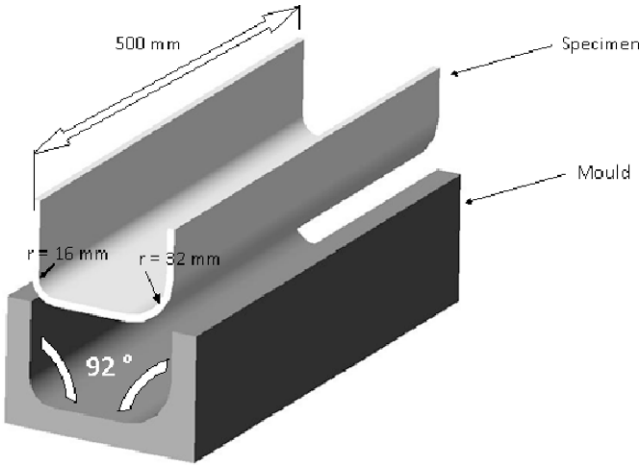

Fig. 2. Geometry of U-channel specimen and tool.

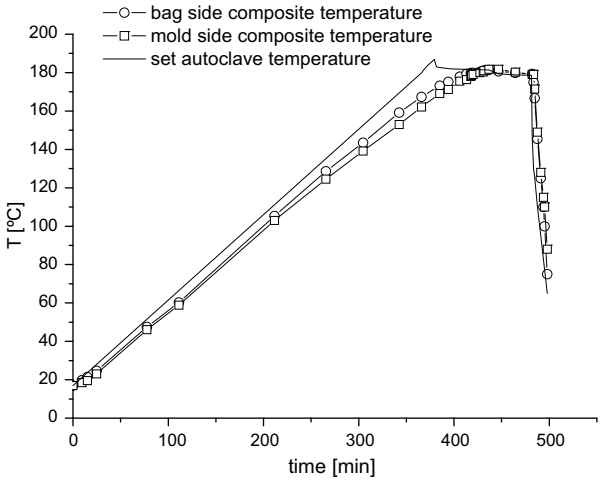

Fig. 3. Autoclave thermal cycle: vessel set temperature (—), bag side material temperature (-o-) and mold side material temperature (-□-).

The CTE was measured by means of TMA 8 Perkin Elmer thermo-mechanical analyzer. TMA tests were performed using a step-wise temperature program between 20 and 200 °C with temperature intervals of 20 °C, raising the temperature between subsequent isothermal steps at 10 °C/min. After reaching the isothermal temperature, the sample was held for 25 min, and then the temperature was raised again to the following test temperature. The force on the sample was held constant to a value of 10 mN, corresponding to about 0.014 bar, at a diameter of the quartz probe of 3 mm. Samples $7 * 8 * 17$ mm were used for in-plane CTE measurement. Samples $7 * 8 * 4$ mm were used for through the thickness CTE measurement. The length of the sample at each temperature was determined as the mean value of the length measured during the last 5 min of the isothermal step. The same temperature program was used without the sample, determining the contribution of quartz probe and support tube to the TMA signal. A base line was built, which was subtracted from the TMA signal, thus determining the dimension of Twintex sample at each temperature.

2.3. Room temperature spring-in angle measurement

The spring-in angle at room temperature, after cooling in the autoclave, was measured by means of an ARES COORD 3 coordinate measuring machine (CMM), equipped with a 40-mm long needle with 2-mm diameter ball. The specimens were fixed on an aluminum plate with epoxy adhesive as shown in Fig. 4. The fixing was conducted taking care not to induce deformation to the sample. A very light veil of glue was placed in edge of each arm to prevent the needle force from moving the specimen. The aluminum plate was screwed to the bed of CMM. The sample was left for 24 h in the CMM room at controlled temperature (20 °C) before measurement. This was done to avoid temperature gradients in the sample, and to allow complete cure of the epoxy.

Six points were recorded on each of the three surfaces of the U-channel, away from the corner radius. A surface was fitted by each group of six point recorded by CMM. Each surface was approximated by the plane best fitting the recorded points, and the angle was determined as the angle enclosed by the planes. The zones used in measurement are shown in Fig. 4. This measurement procedure was repeated along the entire length of U-channel, virtually dividing the specimen into 10 smaller U-channels. The final angle was determined as the average value of the 10 values determined for each U-channel.

The initial spring-in angle $\Delta\theta_i$ was calculated as the difference between the measured angle after consolidation and the set-mould surfaces angle. The set-mold surfaces angle is 92° for both side of the mold as previous described.

The same procedure was followed for each of the two corner radii.

2.4. Thermally induced spring-in angle measurement

A laser measurement technique initially developed by Radford and Rennick and modified in the laboratories of the University of Bristol [23] was used to determine temperature induced angle change during heating (Fig. 5). Sections of U-channel were cut to obtain smaller U-channel 70 mm in length. Two thermocouples were attached on the specimen to monitor the temperature. At each temperature the sample was held for 1 h to avoid temperature gradients in the sample. A small mirror was fixed to the arm of each specimen using wire clips, and another mirror was attached to a fixed support, and used as reference. The deviation of the reflected laser spot from the arm mirror with respect to the reflected laser spot from the fixed mirror was used to determine the angle variation at each temperature.

The geometric parameters used for the determination of the spring-in angle variation are shown in Fig. 6, where β is the angle variation, $(d_1 - d_2)$ is the deviation from initial position of the reflected spot, and $L = 7.3$ m is the distance between projection screen and the mirror on the specimen.

The geometric relationship between β and the others parameter is

$$\beta = \frac{1}{2}\arctan\left(\frac{d_1 - d_2}{L}\right) \tag{1}$$

The spring-in angle variation at each temperature was calculated as $\Delta\theta = \Delta\theta_i - \beta$.

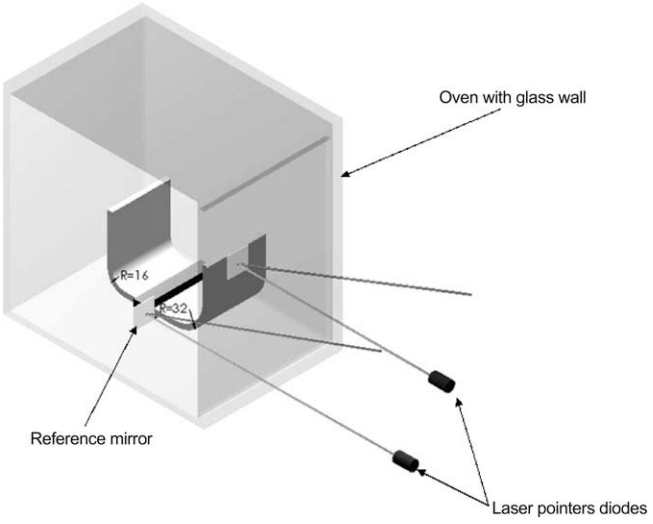

Fig. 5. Laser reflection technique setup.

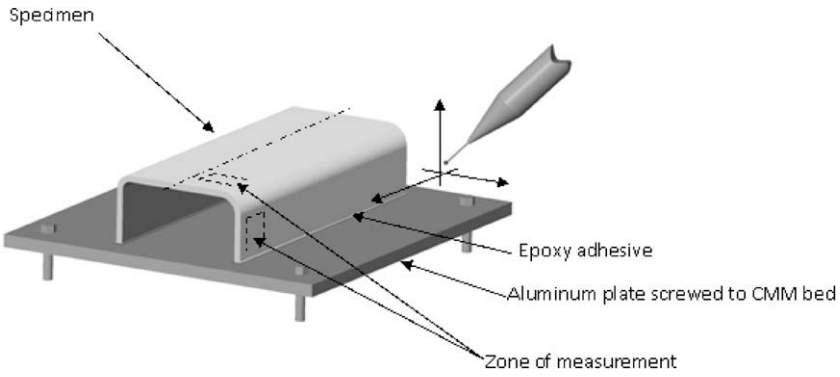

Fig. 4. CMM tests setup for U-channel angles measurement.

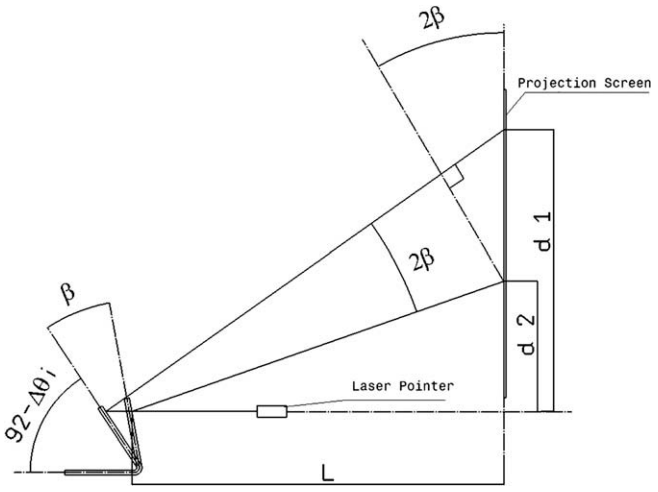

Fig. 6. Scheme of test where β is the angle variation, L is the distance between the specimen and the projection screen, $(d_1 - d_2)$ is the variation in the position of laser reflected spot, 92° is set-mold surfaces angle.

At the end of the heating stage, the sample was cooled back to room temperature. The final spring-in angle $\Delta\theta_f$ was also measured after cooling of the specimen, and the value was compared with the initial value ($\Delta\theta_i$) determined for the sample before heating (cooling hysteresis).

2.5. Density measurement and burn-off test

Density measurement and burn-off test were carried out to evaluate the effect of corner radius on the voids and fibers content of the U-shaped composite. Samples were extracted from each of the corner radii and from the flat zone, as shown in Fig. 7. The burn-off of matrix was carried out on a muffle furnace.

Density measurements were carried out on a Sartorius balance equipped for weighing in water. The density of the specimen and burn-off was performed following ASTM D792 and ASTM D3171-99.

3. Results and discussion

In-plane thermal expansion (parallel to fibers direction) is shown as a function of temperature in Fig. 8. Through thickness thermal expansion is shown as a function of temperature in Fig. 9. As shown in Figs. 8 and 9, the material shows a non-linear expansion behavior in both directions. This indicates a temperature dependence of the CTE, both in the in-plane and through thickness direction. For a non-linear expansion, the evolution of the composite length can be predicted as a function of temperature by applying the exact differential definition of CTE

$$\alpha = \frac{\mathrm{d}\delta}{\delta} \cdot \frac{1}{\mathrm{d}T} \tag{2}$$

where α is the CTE, δ is the characteristic dimension of the composite (in the through the thickness or in-plane direction), T is the temperature. A linear dependence of the CTE upon temperature was assumed for temperatures above the glass transition temperature of the polymer, T_g:

$$\alpha = A + B \cdot (T - T_g) \tag{3}$$

Consequently, after substitution on Eq. (3) into Eq. (2) and integration, each of the characteristic dimension of the composite, δ, can be expressed as a function of temperature as

$$\frac{\delta}{\delta_0} = \exp\left[(A - BT_g)(T - T_0) + \frac{B}{2}(T^2 - T_0^2)\right] \tag{4}$$

where δ_0 and T_0 are the initial values of δ and T.

By non-linear curve fitting of the experimental data reported in Figs. 8 and 9 with Eq. (4), the coefficients A and B were determined in the in-plane and through the thickness directions. Also, the linear fit of experimental parameters, deriving from the assumption of a constant CTE, is reported in Figs. 8 and 9, clearly providing a lower accuracy compared with non-linear curve fit. The values of

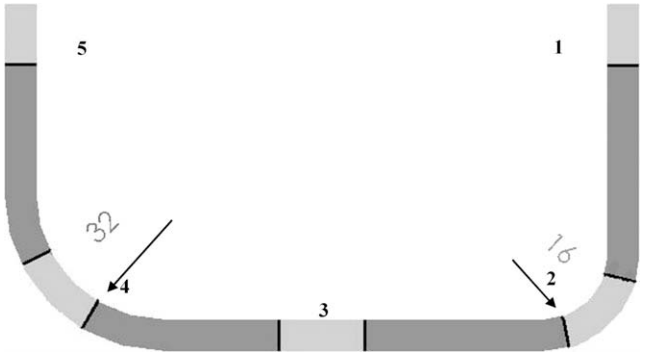

Fig. 7. Specimen for burn-off test from U-section.

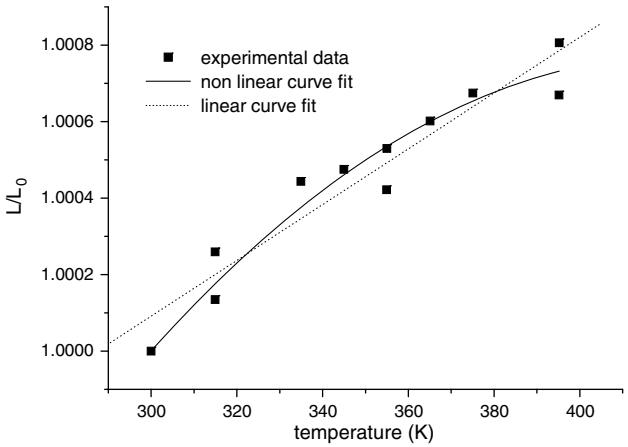

Fig. 8. Results of in-plane CTE evaluation tests: experimental data (■), linear curve fit with constant CTE (—), and non-linear fitting form Eq. (3) (····).

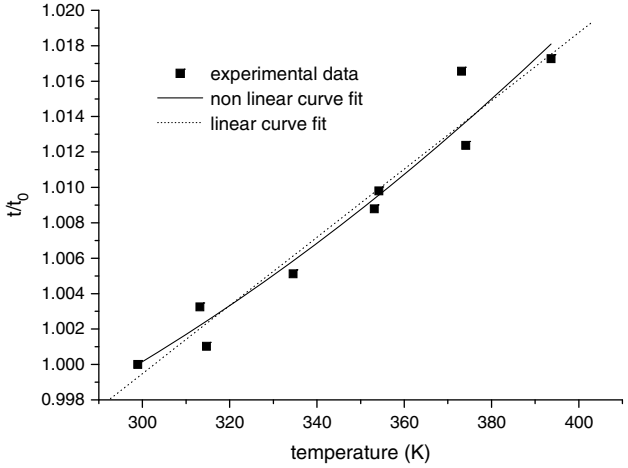

Fig. 9. Results of through the thickness CTE evaluation tests: experimental data (■), linear curve fit with constant CTE (—), and non-linear fitting form Eq. (3) (····).

the coefficients for the temperature dependent and constant CTE determined from regression of experimental data are reported in Table 1.

As expected, the through thickness CTE, which is mainly governed by the polymer matrix CTE, is much higher than the in-plane CTE, which is a property dominated by the glass fiber reinforcement.

The spring-in angle measured at room temperature with a CMM machine after cooling in the autoclave are reported in Table 2, indicated as $\Delta\theta_i$. Results reported in Table 2 indicate that a higher spring-in angle occurs for the smaller inner radius.

Usually, differences in spring-in behavior can be attributed to processing induced defects, including:

- Fibers distortion at the corner, involving an inhomogeneous distribution of resin [23]. The results obtained from resin burn-off tests, reported in Table 3, show some non-homogeneity in the fibers content measured at the corners (specimen 2 and 4 in Fig. 7).

Table 1
In-plane and through thickness CTE parameters for Eq. (3)

	A (K^{-1})	B (K^{-2})	T_g (K)
In-plane CTE	1.628E-5	−1.016E-7	263
In-plane constant CTE	7.29E-6	0	–
Through the thickness CTE	1.169E-4	8.713E-7	263
Through the thickness constant CTE	1.92E-4	0	–

Table 2
Outer corner angles measured by CMM at room temperature after processing

U-channel side	Angle measured 92-$\Delta\theta_i$ (°)	Measured initial spring-in angle $\Delta\theta_i$ (°)	Predicted initial spring-in angle $\Delta\theta_i$ (°) Eq. 6	Density in the corners (g/cm^3)
32-mm outer radius side	90.204	1.796	1.571	1.38
16-mm outer radius side	89.672	2.328	1.571	1.38

Table 3
Burn-off test results

Specimen	Weight% of fibres
1	61.01
2	56.06
3	59.28
4	56.09
5	62.47

- Poor consolidation of the composite at small corner radii. The results reported in Table 2 show that the density of the laminate is homogeneous even in the small corners.
- Fibers wrinkling at corners. Optical microscopy observations shown in Fig. 10a and b show significant misalignment of the fibers accompanied by resin percolation at the corners. In particular, the fibers are better aligned along the circumferential direction for the larger corner radius (Fig. 10a), whereas fibers wrinkling is observed in Fig. 10b) for the smaller radius. Fibers misalignment and resin percolation influence the thermal expansion behavior of the composite, leading to a different spring-in behavior for the two radii.
- Composite thickness non-homogeneities at corners. Even in this case, the results reported in Fig. 10b clearly show that the composite thickness is not homogeneous at smaller corner.

All the process induced defects involve a difference between the actual local CTE of the composite and the measured CTE of the composite, which is evaluated on the flat surfaces specimen. Such effects are more evident at the smaller corner radius, and involve a difference of the spring-in measured for the two corners.

The spring-in angle as a function of temperature measured with the laser technique is reported in Fig. 11 for the 16-mm outer radius, and in Fig. 12 for the 32-mm outer radius. As it can be observed the qualitative behavior of the two curves is similar. The spring-in angle decreases with temperature, with a negative curvature. The negative curvature is due to the temperature dependence of the CTE. Further, for both radii, the final spring-in angle measured after cooling, $\Delta\theta_f$ is much lower than the initial spring-in angle $\Delta\theta_i$. This indicates that significant hysteresis takes place. Hysteresis is attributed to residual stress in the thermally consolidated composite parts, which can relax during the slow heating cycle due to the viscoelastic nature of the polymer matrix.

In order to predict the spring-in angle for the two corner radii, a model derived from the Radford model was used [14]. The original Radford model, which was properly developed for thermoset based composite, assumes that the spring-in angle is only due to composite anisotropy:

$$\Delta\theta = \theta_0 \cdot \left(\frac{(\alpha_l - \alpha_t)\Delta T}{1 + \alpha_t \Delta T}\right) + \theta_0 \cdot \left(\frac{\phi_l - \phi_t}{1 + \phi_t}\right) \tag{5}$$

where $\Delta\theta$ is the spring-in angle, θ_0 is the initial included angle of the component, α_l is the in-plane CTE, α_t is the through the thickness CTE, ΔT is the temperature change, ϕ_l is the in-plane cure shrinkage, ϕ_t is the through the thickness cure shrinkage.

In the case of thermoplastic matrix composite the spring-in develops during the cooling stage. As a consequence, the cure

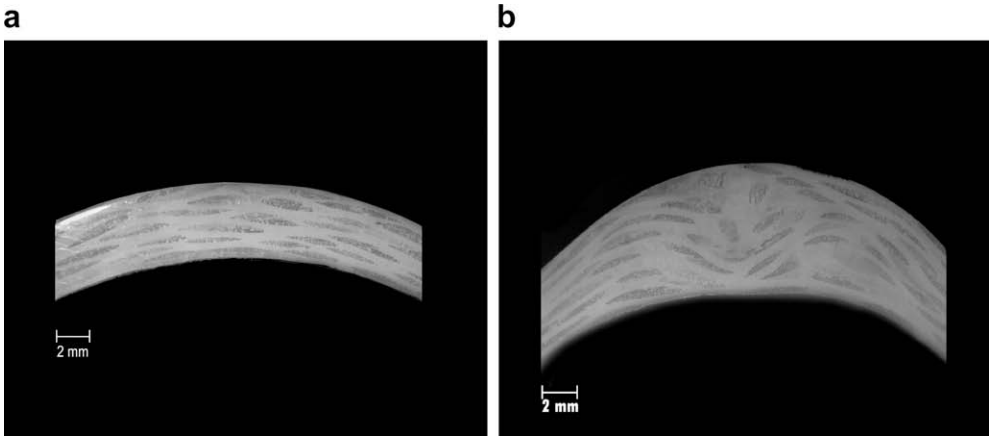

Fig. 10. Optical microscopy images for 32 mm (a), and 16 mm (b) corner radius.

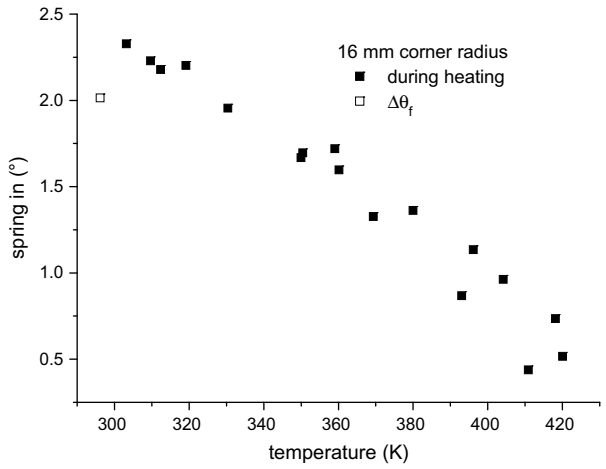

Fig. 11. Experimental spring-in angle variation ($\Delta\theta_i - \beta$) for the 16-mm corner radius during heating (■) and after cooling ($\Delta\theta_f$) (□).

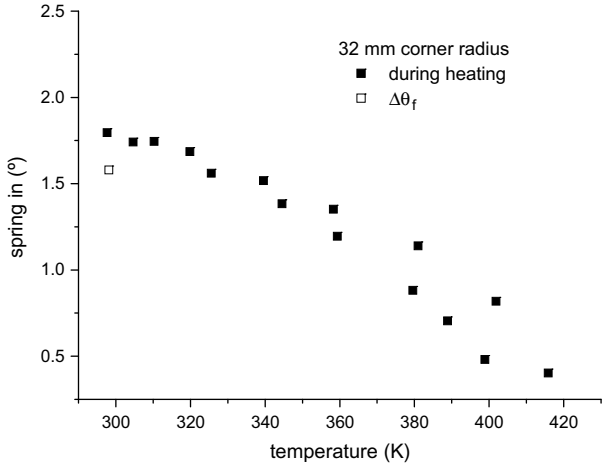

Fig. 12. Experimental spring-in angle variation ($\Delta\theta_i - \beta$) for the 32-mm corner radius during heating (■) and after cooling ($\Delta\theta_f$) (□).

shrinkage can be substituted by the crystallization shrinkage. Nevertheless, for thermoplastic matrix composite, no spring-in can occur before crystallization, when the polymer is in the molten phase. As a consequence of this, the second contribution on the right hand side of Eq. (5) can be neglected.

Therefore, the Radford model can be rewritten as reported in Eq. (6):

$$\Delta\theta = \theta_0 \cdot \left(\frac{(\alpha_l - \alpha_t)\Delta T}{1 + \alpha_t \Delta T}\right) \tag{6}$$

For the materials studied, as $\alpha_l << \alpha_t$, and $\alpha_t \Delta T << 1$, the Radford model can be further approximated as:

$$\Delta\theta = -\theta_0 \alpha_t \Delta T \tag{7}$$

The simplified model, as well as the original Radford model, is only valid if the CTE is not temperature dependent. For the Twintex composite, the temperature dependence of both CTE requires the use of the differential form of Eq. (7). Using the expression for $\Delta\theta = \theta_0 - \theta$, the differential form of Eq. (7) can be obtained as:

$$d\theta = \theta \alpha_t dT \tag{8}$$

By substitution of Eq. (3) into Eq. (8) and integration, the evolution of the angle as function of temperature can be obtained, as reported in Eq. (9):

$$\frac{\theta}{\theta_0} = \exp\left(\left[(A - BT_g)(T - T_0) + \frac{B}{2}(T^2 - T_0^2)\right]\right) \tag{9}$$

Finally, the values of spring-in angle $\Delta\theta$ can be obtained as

$$\Delta\theta = \theta_0\left(1 - \exp\left(\left[(A - BT_g)(T - T_0) + \frac{B}{2}(T^2 - T_0^2)\right]\right)\right) \tag{10}$$

Although the composite is processed at 180 °C, assuming that no spring-in occurs before crystallization of the polymer matrix, the initial temperature for spring-in angle development can be assumed to be equal to the onset of crystallization. The DSC analysis of the composite during cooling is reported in Fig. 13, showing that the onset of crystallization is about 116 °C. The DSC cooling scan was performed at 6.5 °C/min which is a cooling rate equal to that measured during autoclave processing.

A comparison between experimental data for spring-in as a function of temperature and model prediction according to Eq. (10) is shown in Fig. 14 for the 16-mm corner and in Fig. 15 for the 32-mm corner. Also, for comparison purposes, the model prediction according to Eq. (10) with the constant CTE values of Table 1 are reported. As it can be observed, the model prediction with temperature dependent CTE are in better agreement with experimental data.

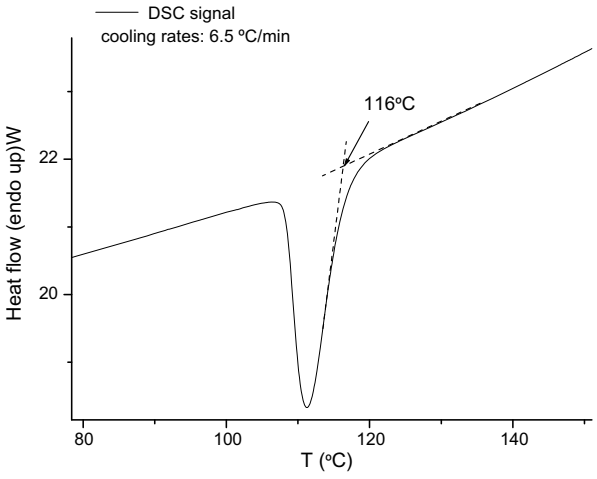

Fig. 13. Crystallization peak of Twintex by DSC analysis.

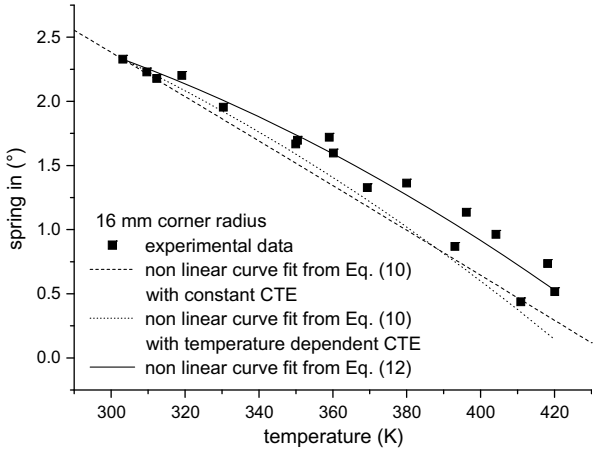

Fig. 14. Comparison of experimental spring-in for 16 mm corner radius (■), model prediction according to Eq. (10) with constant CTE (- - -) and with temperature dependent CTE (····), and model prediction according to Eq. (12) (—).

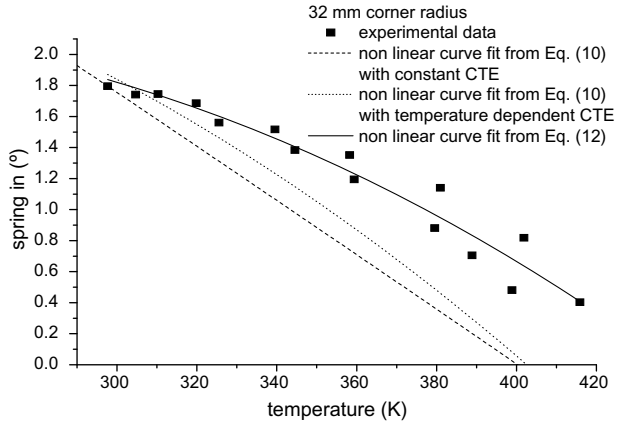

Fig. 15. Comparison of experimental spring-in for 32 mm corner radius (■) model prediction according to Eq. (10) with constant CTE (- - -) and with temperature dependent CTE (····), and model prediction according to Eq. (12) (—).

Some differences between the experimental and model predicted spring-in angle can be observed in the three different phases of the temperature evolution of each sample.

During cooling inside the autoclave the spring-in angle should increase with decreasing temperature according to Eq. (10). Assuming that the spring-in angle is zero at the onset temperature of crystallization, the spring-in angle after cooling in the autoclave, determined from Eq. (10), can be evaluated to be 1.571°, which is slightly different from the experimental values as reported in Table 2. The difference between experimental and analytical data can be attributed to the fact that the spring-in angle evolution during the autoclave cycle is not free, being constrained by the externally applied pressure and the female tool. Also, the difference between the theoretical spring-in value and the smaller corner spring-in is much higher than the difference between the theoretical value and the higher corner spring-in. This indicates that the differences observed are also a consequence of the processing induced defects previously discussed, which become more relevant for the smaller corner.

During the subsequent heating, the spring-in angle decreases with temperature, as reported in Figs. 11 and 12. Also, model prediction data are reported in Figs. 14 and 15. In both cases, the model is able to predict the qualitative behavior of the spring-in. Nevertheless, significant differences exist, attributed to processing induced defects.

During subsequent cooling, the spring-in angle value should be equal to the initial spring-in angle determined at the beginning of heating. The different behavior reported in Figs. 11 and 12 indicates the relevance of non-thermoelastic effects, as previously discussed.

In order to obtain a better fit of experimental data, the Radford model was modified to account for the presence of fibers wrinkling at corner radii. According to the results reported in Fig. 10a and b, the fibers misalignment and resin percolation should involve a decrease of the CTE in the through the thickness direction, and conversely an increase of the CTE in the in-plane direction. In both cases, it is possible to account for such effects by considering a corrective CTE, α_c, which is subtracted by the through the thickness CTE. Accordingly, the differential form of the Radford model can be written as:

$$d\theta = \theta(\alpha_t - \alpha_c)dT \tag{11}$$

And by integration, assuming that α_c is not temperature dependent, and accounting for the temperature dependence of α_t, the following expression can be obtained for the spring-in:

$$\Delta\theta = \theta_0\left(1 - \exp\left(\left[(A - BT_g - \alpha_c)(T - T_0) + \frac{B}{2}(T^2 - T_0^2)\right]\right)\right) \tag{12}$$

A comparison between the experimental and model prediction according to Eq. (12) is reported in Fig. 14 for the 16-mm corner radius and in Fig. 15 for the 32-mm corner radius. The values of α_c are $6.86 * 10^{-5}$ and $3.58 * 10^{-5}\,K^{-1}$ for the higher and the smaller corners, respectively. As it can be observed, the introduction of the corrective factor significantly increases the accuracy of the model prediction. This indicates that processing induced defects, resulting in an increase of the in-plane CTE and a decrease of the through the thickness CTE, play a significant role in determining the spring-in behavior of thermoplastic matrix composites.

4. Conclusions

In this work, the spring-in angle of thermoplastic based commingled composite Twintex PP has been studied. U-channel shaped and flat laminates specimens were obtained by vacuum molding and autoclave curing. TMA analysis was used to determine the thermal expansion coefficients of the composite in the through the thickness and the in-plane directions, showing that the through the thickness direction CTE is much higher than the in-plane CTE.

The anisotropic thermal expansion behavior of the composite results in spring-in of the U-shaped laminate when it is subjected to temperature variations.

In particular, it was shown that during cooling the composite experiences spring-in, as evidenced by CMM measurements. During subsequent heating of the composite, spring-out is observed. These results indicate that the spring-in behavior of the thermoplastic based composite is similar to that of traditional thermoset based composite. Nevertheless, significant differences were observed for the two corner radii. The observed differences can be attributed to processing defects of the composite, which are more evident at the smaller corner, including:

- inhomogeneous fibers distribution at corners;
- fibers wrinkling at corners;
- composite thickness non-homogeneities at corners.

In order to predict the spring-in behavior of the thermoplastic matrix composite, a model derived from the Radford model was applied.

The Radford model was able to capture the qualitative behavior of the composite. In order to obtain a good fit of the experimental data, the Radford model was modified to account for the CTE variations at corners due to fibers wrinkling.

Besides to this, the thermoplastic matrix composite shows non-thermoelastic effects which cannot be predicted by the Radford model. Such effects are evidenced as an hysteresis of the spring-in, which is much lower, for both corner radii, after heating of the material and subsequent cooling. The heating and cooling cycle after processing can induce structural modifications of the polymer matrix as well as viscous stress relaxations. This obviously indicates that for thermoplastic matrix composite the spring-in angle behavior can also depend on the holding time of the material at high temperatures, which in turn mainly depend on the cooling rate during processing. For faster processes a more relevant effect of residual stresses on spring-in angle is expected. This could also result from a lower degree of crystallinity due to higher cooling rates. However, the residual stresses should be lower if an amorphous matrix is used, thanks to its lower relaxation times.

References

[1] Pegoretti A, Ricco T. Creep crack growth in a short glass fibres reinforced polypropylene composite. J Mater Sci 2001;36:4637–41.
[2] Corvaglia P, Passaro A, Manni O, Barone L, Maffezzoli A. Recycling of PP-based sandwich panels with continuous fibers composite skins. J Thermoplast Compos 2006;19:731–45.

[3] Greco A, Maffezzoli A. Statistical and kinetic approaches for LLDPE melting modeling. J Appl Polym Sci 2003;89:289–95.
[4] Wysocki M, Larsson R, Toll S. Hydrostatic consolidation of commingled fibre composites. Compos Sci Technol 2005;65:1507–19.
[5] Long AC, Wilks CE, Rudd CD. Experimental characterisation of the consolidation of a commingled glass/polypropylene composite. Compos Sci Technol 2001;61:1591–603.
[6] Ye L, Friedrich K, Kastel J, May YW. Consolidation of unidirectional CF/PEEK composites from commingled yarn prepreg. Compos Sci Technol 1995;54:349–58.
[7] Bates PJ, Taylor D, Cunningham MF. Compaction and transverse permeability of glass rovings. Appl Compos Mater 2001;8:163–78.
[8] Passaro A, Corvaglia P, Manni O, Barone L, Maffezzoli A. Processing-properties relationship of sandwich panels with polypropylene-core and polypropylene-matrix composite skins. Polym Composite 2004;25(3):307–18.
[9] Torre A, Maffezzoli A, Kenny JM. A macrokinetic approach to crystallization applied to New TPI (Thermoplastic Polyimide) as a model polymer. J Appl Polym Sci 1995;56:985–93.
[10] Torre L, Kenny JM, Recca A, Siracusa V, Tarzia A, Maffezzoli A. Crystallization of an aromatic Poly-ether-ketone (PK99) by calorimetric and X-ray analysis. J Therm Anal 2000;61:565–78.
[11] Phillips R, Devrim A, Manson JAE. Prediction of the consolidation of woven fibre-reinforced thermoplastic composites. Part I. Isothermal case. Compos Part A-Appl S 1998;29A:395–402.
[12] Michaud VJ, Manson JAE. Impregnation of compressible fiber mats with a thermoplastic resin. Part I: theory. J Compos Mater 2001;35:1150–73.
[13] Albert C, Fernlund G. Spring-in and warpage of angled composite laminates. Compos Sci Technol 2002;62:1895–912.
[14] Radford DW, Rennic TS. Separating sources of manufacturing distortion in laminated composites. J Reinf Plast Comp 2000;19(8):621–41.
[15] Lalit K J, Meng H, Lin Y, Yiu-Wing M. Spring-in study of the aileron rib manufactured from advanced thermoplastic composite. Compos Part A-Appl S 1998;29A:973–9.
[16] Ersoy N, Potter K, Wisnom MR, Clegg MJ. Development of spring-in angle during cure of a thermosetting composite. Composites: Part A 2005;36:1700–6.
[17] Huang CK, Yang SY, Chen CC. Influence of processing on warpage of composite parts. J Adv Mater 2005;37(4):17–22.
[18] Jain LK, Hou M, Ye L, Mai YW. Spring-in study of the aileron rib manufactured from advanced thermoplastic composite. Compos Part A-Appl S 1998;29(8):973–9.
[19] Kim BS, Bernet N, Sunderland P, Manson JA. Numerical analysis of the dimensional stability of thermoplastic composites using a thermoviscoelastic approach. J Compos Mater 2002;36(20):2389–403.
[20] Bapanapalli SK, Smith LV. A linear finite element model to predict processing-induced distortion in FRP laminates. Compos Part A-Appl S 2005;36(12):1666–74.
[21] Parlevliet PP, Bersee HEN, Beukers A. Residual stresses in thermoplastic composites – A study of the literature – Part I: formation of residual stresses. Compos Part A-Appl S 2006;37(11):1847–57.
[22] Salomi A, Greco A, Maffezzoli A, et al. A preliminary study on bladder-assisted rotomolding of thermoplastic polymer composites. Advances in Polymer Technology 2007;26(1):21–32.
[23] Thomasz Garstka. PhD Thesis. Separation of process induced distortions in curved composite laminates, University of Bristol, 2005.